J Biol Inorg Chem (2006) 11: 609–616
DOI 10.1007/s00775-006-0110-0

ORIGINAL PAPER

Pablo J. González · María G. Rivas
Carlos D. Brondino · Sergey A. Bursakov
Isabel Moura · José J. G. Moura

EPR and redox properties of periplasmic nitrate reductase from *Desulfovibrio desulfuricans* ATCC 27774

Received: 9 February 2006 / Accepted: 13 April 2006 / Published online: 9 May 2006

Abstract Nitrate reductases are enzymes that catalyze the conversion of nitrate to nitrite. We report here electron paramagnetic resonance (EPR) studies in the periplasmic nitrate reductase isolated from the sulfate-reducing bacteria *Desulfovibrio desulfuricans* ATCC 27774. This protein, belonging to the dimethyl sulfoxide reductase family of mononuclear Mo-containing enzymes, comprises a single 80-kDa subunit and contains a Mo bis(molybdopterin guanosine dinucleotide) cofactor and a [4Fe–4S] cluster. EPR-monitored redox titrations, carried out with and without nitrate in the potential range from 200 to −500 mV, and EPR studies of the enzyme, in both catalytic and inhibited conditions, reveal distinct types of Mo(V) EPR-active species, which indicates that the Mo site presents high coordination flexibility. These studies show that nitrate modulates the redox properties of the Mo active site, but not those of the [4Fe–4S] center. The possible structures and the role in catalysis of the distinct Mo(V) species detected by EPR are discussed.

Keywords Molybdenum-containing enzymes · Periplasmic nitrate reductase · Dimethyl sulfoxide reductase family · Electron paramagnetic resonance · Redox titration

Abbreviations *Dd*: *Desulfovibrio desulfuricans* ATCC 27774 · *Ec*: *Escherichia coli* K12 · EPR: Electron paramagnetic resonance · Euk-NR: Eukaryotic nitrate reductase · EXAFS: Extended X-ray absorption fine structure · Fdh: Formate dehydrogenase · Mo-bisMGD: Mo bis(molybdopterin guanosine dinucleotide) · MV: Methyl viologen · Nas: Assimilatory nitrate reductase · Nap: Periplasmic nitrate reductase · Nar: Respiratory nitrate reductase · NHE: Normal hydrogen electrode · NR: Nitrate reductase · *Pp*: *Paracoccus pantotrophus* · *Rs*: *Rhodobacter sphaeroides* · Tricine: *N*-Tris(hydroxymethyl)methylglycine · Tris: Tris(hydroxymethyl)aminomethane

Introduction

Nitrate reduction occurs in the cell in order to incorporate nitrogen into biomolecules (assimilatory ammonification) as the final electron acceptor when bacteria are grown in anaerobic conditions (denitrification) and to eliminate energy excess generated by the cell metabolism (dissimilatory ammonification) [1–3]. Nitrate reductases (NRs) are enzymes that catalyze the reduction of nitrate according to the reaction:

$$NO_3^- + 2H^+ + 2e^- \rightarrow NO_2^- + H_2O \quad E^o = +420\,mV.$$

Most NRs are mononuclear molybdenum-containing enzymes present in several living organisms which have, in addition to a molybdenum active site, additional redox cofactors such as iron–sulfur and heme centers that mediate electron transfer reactions between the electron donor and the nitrate [4]. NRs have been classified into four groups according to different

Electronic Supplementary Material Supplementary material is available for this article at http://dx.doi.org/10.1007/s00775-006-0110-0 and is accessible for authorized users.

P. J. González · M. G. Rivas · S. A. Bursakov · I. Moura
J. J. G. Moura (✉)
REQUIMTE/CQFB,
Departamento de Química,
Faculdade de Ciências e Tecnologia,
Universidade Nova de Lisboa,
2829-516 Caparica, Portugal
E-mail: jose.moura@dq.fct.unl.pt
Tel.: +351-21-2948382
Fax: +351-21-2948550

C. D. Brondino (✉)
Facultad de Bioquímica y Ciencias Biológicas,
Universidad Nacional del Litoral,
3000 Santa Fe, Argentina
E-mail: brondino@fbcb.unl.edu.ar
Tel.: +54-342-4575213
Fax: +54-342-4575221

criteria, such as localization of the enzyme in the cell, molecular properties of the catalytic center, and source: (1) eukaryotic NRs (Euk-NRs), (2) assimilatory NRs (Nas), (3) respiratory NRs (Nar), and (4) periplasmic NRs (Nap) [5, 6]. Nas, Nar, and Nap, which are only found in prokaryotic organisms, belong to the dimethyl sulfoxide reductase family, whereas Euk-NRs belong to the sulfite oxidase family of molybdo proteins [4]. Euk-NR and Nas are cytoplasmic enzymes involved in nitrate assimilation, whereas Nar are membrane-bound enzymes involved exclusively in denitrification. In contrast, Nap is the only example with a not well defined function. This was concluded from the fact that its maximal expression varies between the species and no transcription promoter or conserved DNA consensus related to the nitrogen metabolism have been found in all the operons that encode them [1]. Therefore, physiological functions such as minimization of the reducing power under certain conditions of growth [7–12], denitrification [13–16], and scavenging nitrate when it is limited in the medium [17] have been proposed for these enzymes. In contrast to most denitrifying bacteria, the sulfate reducer *Desulfovibrio desulfuricans* ATCC 27774 (*Dd*) has Nap as the only NR activity. This enzyme is expressed when nitrate is used as the final electron acceptor in anaerobic conditions [15], as in the case of Nar from denitrifying organisms. This implies that Nap is used as a respiratory system and, like Nap from *Escherichia coli* K12 (*Ec* Nap), nitrate reduction should be coupled to a proton electrochemical gradient generated by using the quinone pool [18, 19].

Naps from *Dd*, *Paracoccus pantotrophus* (*Pp*), and *Rhodobacter sphaeroides* (*Rs*) constitute the best-characterized Naps, so far. The 3D X-ray structure of *Dd* NapA was the first reported for a Nap enzyme [20]. This is a monomeric protein with a funnel-like cavity formed from the surface to the active site (approximately 15 Å), which is suggested to be the path for nitrate entrance and nitrite exit. The active site is a Mo bis(molybdopterin guanosine dinucleotide) (Mo-bisMGD) cofactor and, in addition, there is a [4Fe–4S] cluster, likely involved in the electron transfer. *Rs* NapAB [21] and *Pp* NapAB [22] are heterodimeric proteins, but with their catalytic subunits closely related to *Dd* NapA. The structures of the catalytic subunits of *Dd* NapA [20] and *Rs* NapA [23] are very similar in terms of metal cofactor content, global fold, and domain organization. Although the primary sequences of *Dd* NapA reveal a low identity (approximately 35%) with *Rs* NapA and *Pp* NapA, the residues involved in both Mo-bisMGD cofactor and [4Fe–4S] cluster binding are conserved [24]. The active site in the oxidized forms of *Dd* NapA and *Rs* NapAB is formed by a distorted hexa-coordinated Mo(VI) ion, in which the metal atom is coordinated by four sulfur atoms from two dithioline ligands, one hydroxo/water group, and S_γ from Cys_{140} (in *Dd* NapA numbering) [20]. In contrast, on the basis of electron paramagnetic resonance (EPR) and extended X-ray absorption fine structure (EXAFS) studies, a hepta-coordinated molybdenum site was postulated for *Pp* NapAB [25], in which an additional oxo group constitutes the main difference from the oxidized active sites of *Dd* NapA and *Rs* NapAB [20, 23], whereas a negatively charged hepta-coordinated complex was proposed for the reduced form. The structure of the reduced active site in *Dd* NapA and *Rs* NapAB has not been reported. However, a penta-coordinated Mo(IV) site in which the apical position is occupied by S_γ of Cys_{140} was postulated on the basis of the high homology between *Dd* NapA and *Ec* Fdh-H, where Fdh is formate dehydrogenase [24].

The EPR studies of *Pp* NapAB reveal Mo sites with a high flexibility of coordination as demonstrated from the several EPR signals obtained in different experimental conditions. Particularly, nitrate addition to a dithionite-reduced sample yields an EPR signal called *high g* (nitrate), which was postulated to be produced by a catalytic intermediate of the reaction [25]. Previous EPR characterization of *Dd* NapA also detected a similar EPR signal [26] that develops upon nitrate addition to a dithionite-reduced sample. In order to address the catalytic competence of this signal, the structure of the EPR-active species, and to evaluate the redox properties of the metal cofactors in *Dd* NapA, we performed EPR-monitored redox titrations with and without nitrate. EPR studies with the enzyme in both catalytic and inhibited conditions are also reported.

Experimental

Cell growth and protein purification

The *Dd* cells were grown as described previously [27], harvested in 10 mM tris(hydroxymethyl)aminomethane (Tris)-HCl pH 7.60, and passed through a Manton-Gaulin press at 9,000 psi. The cell debris was centrifuged at 16,000*g* for 30 min. In order to obtain the soluble fraction, the supernatant was ultracentrifuged at 180,000*g* for 1 h. Purification of *Dd* NapA up to electrophoretic grade was carried out through a four-step protocol, which has some modifications with respect to the previous ones [15, 26]. The soluble extract was loaded into a (diethylamino)ethyl-cellulose column equilibrated with 10 mM Tris-HCl pH 7.6. *Dd* NapA was eluted at 75–100 mM buffer molarity of the gradient. The fractions containing NR activity were pooled, dialyzed against 10 mM Tris-HCl pH 7.6, and loaded into a Q-Sepharose column. After elution, fractions containing NR activity were pooled and loaded into a hydroxyapatite column equilibrated with 100 mM Tris-HCl pH 7.6 and were eluted with a potassium phosphate linear gradient. The pool containing *Dd* NapA was dialyzed against 5 mM phosphate buffer pH 8.0, and was loaded into a Resource Q (Pharmacia) column. *Dd* NapA was

eluted with a linear gradient in the 15–20 mM buffer. All purification procedures were performed at 277 K under aerobic conditions.

Enzyme assays and protein determination

Enzymatic assays were performed by the discontinuous method determining accumulated nitrite as previously described [26], but with some modifications. The enzyme was preincubated for 10 min at 303 K with a solution containing 100 mM Tris–HCl pH 7.6, 5 mM methyl viologen (MV), and 5 mM sodium dithionite. The reaction was started by the addition of the substrate and was allowed to proceed for 30 s. The total protein concentration was determined using both the extinction coefficient ($\varepsilon_{400\ nm} = 24\ mM^{-1}\ cm^{-1}$) and the bicinchoninic acid kit from Sigma.

EPR spectroscopy

X-band spectra were recorded with a Bruker EMX spectrometer equipped with a dual-mode cavity (model ER4116DM) and an Oxford Instruments continuous-flow cryostat. Simulations were performed using the WIN-EPR Simfonia V1.2 software from Bruker Instruments. All the samples were prepared in 100 mM *N*-tris (hydroxymethyl)methylglycine (Tricine) pH 8.0 with a protein concentration of 200 μmol dm^{-3}. All the spectra were obtained in nonsaturating conditions at 25 and 100 K. For the spectra taken at 25 K, the experimental conditions were as follows: microwave power, 0.6 mW; modulation amplitude, 5 G. For the spectra taken at 100 K, unless otherwise stated, the conditions were the same except for a microwave power of 2 mW. Spin quantification of the Mo(V) and FeS signals was estimated by double integration and comparison with a 1 mM Cu EDTA standard.

Spectropotentiometric titration

Redox titrations were carried out in an anaerobic chamber at room temperature working at an oxygen concentration below 1 ppm. A platinum–silver/silver chloride combined electrode (Crison) was used to determine the electrochemical potential. The samples were incubated with the mediators MV (−440 mV), neutral red (−325 mV), anthroquinone (−225 mV), fenazine (−125 mV), indigotetrasulfonic acid (−46 mV), duroquinone (5 mV), galocyanine (30 mV), fenazine etasulfate (55 mV), fenazine metasulfate (80 mV), 2,5-dimethyl benzoquinone (180 mV), and 2,6-dichlorophenol indophenol (217 mV). The electrochemical potential was dropped using a sodium dithionite (40 mg ml^{-1}) solution dissolved in 100 mM Tricine pH 8.0. Samples for EPR spectroscopy were taken after equilibration at each potential and were frozen in liquid nitrogen. EPR spectra were recorded at 25 and 100 K as described already.

Results

EPR spectroscopy of as-prepared, dithionite-reduced and nitrate-oxidized samples

The EPR spectrum taken of the as-prepared enzyme (Fig. 1, spectrum a) shows a signal observable with no significant broadening up to 150 K (*resting* signal). Both temperature variation and g values are compatible with Mo(V) ions (less than 0.05 spins per molecule). The broad component in the g_1 region suggests the presence of unresolved splitting(s) by nonexchangeable protons with solvent, likely from backbone or amino acid side chains, since this signal does not alter upon D_2O exchange. This signal disappears after reduction with dithionite and cannot be restored after air oxidation.

Figures 1, spectrum b and 2, spectrum a show the spectra obtained after anaerobic dithionite reduction (20-fold molar excess). The low-temperature spectrum (Fig. 2, spectrum a) is the superimposition of the EPR signal associated with the $[4Fe–4S]^{+}$ center and a less intense rhombic signal due to Mo(V) ions, which is observed without broadening up to 150 K and accounts for 0.15 spins per molecule (Fig. 1, spectrum b), which corresponds to the maximum value found in samples from several purification batches. This Mo(V) species (hereafter named *low-potential* species) has a lower

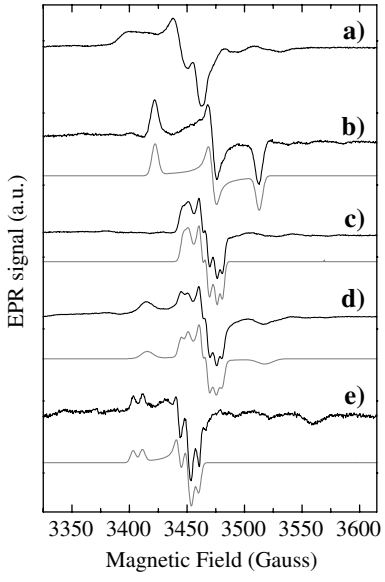

Fig. 1 Mo(V) electron paramagnetic resonance (*EPR*) spectra obtained for *Desulfovibrio desulfuricans* ATCC 27774 (*Dd*) periplasmic nitrate reductase A (*NapA*) at 100 K together with the simulation (*gray lines*). *a* As-prepared sample, *b* as-prepared sample reduced with 5 mM sodium dithionite, *c* same as for *b*, but after addition of 100 mM sodium nitrate, *d* same as for *c*, but oxidized with air, and *e* same as for *b*, but with 20 mM cyanide added and followed by air oxidation. The EPR parameters used in the simulation are given in Table 1

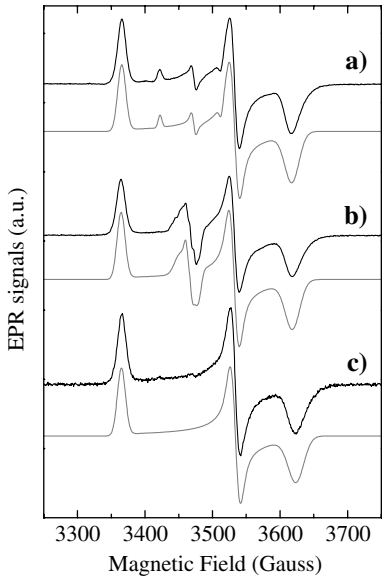

Fig. 2 Low-temperature (25 K) EPR spectra of *Dd* NapA samples together with simulation (*gray lines*). *a* Sample reduced with 5 mM sodium dithionite, *b* same as for *a* after adding 100 mM sodium nitrate, and *c* same as for *a*, but containing 20 mM cyanide and reoxidized with air. The EPR parameters used in the simulation of the FeS center signal were $g_1 = 2.049$ (12 G), $g_2 = 1.952$ (12 G), and $g_3 = 1.906$ (21 G) for spectra *a* and *b* (linewidths in parentheses). The parameters for spectrum *c* were the same except $g_3 = 1.903$ (23 G). The parameters used for Mo(V) signals are given in Table 1

midpoint redox potential (less than −500 mV vs. the normal hydrogen electrode, NHE, see later) than the resting species. The low-potential signal shows no significant differences when D_2O-exchanged samples are used (not shown) but, in contrast to the resting signal and other EPR signals discussed later, no evidence for hyperfine coupling with nuclei with $I = 1/2$ can be found. This signal has not been observed in other NRs and resembles the one called *rhombic II* in *Dd* Fdh (*g* values in Table 1), which is also obtained upon dithionite reduction [28].

Addition of nitrate (500-fold molar excess) to the dithionite-reduced sample does not affect the FeS signal (Fig. 2, spectrum b), which is consistent with the fact that this cofactor acts as an electron transfer center. However, as reported before [26], nitrate addition in anaerobic conditions to dithionite-reduced samples of *Dd* NapA yields the Mo(V) EPR signal of Fig. 1, spectrum c. This signal shows hyperfine splitting with a species with nuclear spin $I = 1/2$, which is not exchangeable with solvent. The intensity increases with both the nitrate concentration and the incubation time, reaching a maximum of 40% of the total molybdenum after 40 min at a nitrate concentration of 0.1 mol dm^{-3}. The same spectrum was also obtained after air oxidation of a dithionite-reduced sample but had a lower intensity compared with that obtained with nitrate oxidation (less than 10%). Although nitrate is not essential to produce this signal, it will be called the *nitrate* signal (EPR parameter in Table 1).

Exposure to air of a sample showing the nitrate signal oxidizes the FeS center to the diamagnetic state $[4Fe–4S]^{2+}$ but leaves the intensity of the *nitrate* signal unaffected, suggesting that the resulting Mo(V) species is stabilized after nitrate addition. As seen in Fig. 1, spectrum d, this procedure also produces an additional rhombic Mo(V) signal, which will be named *high potential* as it is produced in the presence of oxygen (redox potential approximately 200 mV vs. NHE), and is identical to the rhombic I signal reported in *Dd* Fdh (*g* values in Table 1) [28]. However, this signal was not observed in all the cases analyzed and its observation depends on the batch of enzyme utilized in each experiment.

Spectropotentiometric titration

In order to evaluate the redox properties of the different Mo(V) species and the FeS center, we performed spec-

Table 1 Electron paramagnetic resonance (*EPR*) parameters of the Mo(V) species found in *Desulfovibrio desulfuricans* ATCC 27774 (*Dd*) periplasmic nitrate reductase (*NapA*) and related mononuclear molybdenum-containing enzymes

Enzyme	EPR signal	g_1	g_2	g_3	A_1	A_2	A_3
Dd NapA (this work)	*Low potential*	2.016 (5.5)	1.987 (5.5)	1.964 (5.5)	–	–	–
	High potential	2.019 (5.5)	1.988 (5.5)	1.960 (5.5)	–	–	–
	Nitrate	2.000 (4.4)	1.990 (3.6)	1.981 (3.4)	4.6	5.0	4.6
	Turnover $^{14}N/^{15}N$	1.999 (5.0)	1.990 (5.0/4.0)	1.982 (5.0/4.0)	5.0	6.0	5.0
	Cyanide	2.024 (4.5)	2.001 (4.0)	1.995 (4.0)	8.0	7.5	6.0
Pp NapAB [25]	*High g (resting)*	1.999	1.989	1.982	6.4/3.2	4.3	4.6
	High g (nitrate)	1.997	1.990	1.982	6.5/2.2	6.0	5.0
	Very high g (cyanide)	2.022	1.999	1.994	7.4	7.4	6.6
Dd Fdh [28]	*Rhombic I*	2.019	1.988	1.963	–	–	–
	Rhombic II	2.009	1.984	1.951	–	–	–
Mf Fdh [36]	*Reduced*	2.005	1.998	1.989	10.5	8.5	8.8
Ssp NarB [29]	*Air-oxidized*	2.023	1.998	1.993	6.8	7.5	6.8

The values in *parentheses* for *Dd* NapA are the linewidths used in the simulation of the spectra shown in Fig. 1. The hyperfine parameters (*A*) and linewidths are in gauss

Pp Paracoccus pantotrophus, *Fdh* formate dehydrogenase, *Mf Methanobacterium formicicum*, *Ssp Synechococcus* sp. PCC 7942, *Nar* respiratory nitrate reductase

tropotentiometric titrations in the potential range from 150 mV (a value where the electrochemical potential stabilizes without dithionite addition) to −500 mV. Figure 3 shows the relative intensity for the *low-potential* species and the FeS center EPR signal as a function of the electrochemical potential of the solution. The *resting* signal, which was detected for the as-prepared samples, was not observed in this experiment. A least-squares fit to the data of the FeS signal with a Nernstian function ($n=1$) yielded $E=-390$ mV (vs. NHE). This value is unusually low for Naps, which usually have FeS centers with redox potentials around −200 mV [23, 25, 29]. The redox potentials of the low-potential species could not be precisely determined owing to the lack of data below −500 mV (Fig. 3). The intensity of the *low-potential* signal accounted for approximately 0.05 spins per molecule at the lowest potential reached in this experiment. This value is far from the value of approximately 0.3 spins per molecule that should be obtained in the hypothetical situation of identical midpoint redox potentials for the couples Mo(VI)/Mo(V) and Mo(V)/Mo(IV) (it was assumed to be −500 mV for both redox couples). This indicates that the Mo(V)/Mo(IV) redox pair has an even more negative redox potential, which confirms that the molybdenum cannot be completely reduced to Mo(IV) on dithionite reduction.

In order to evaluate the redox potential of the *nitrate* species, the redox titration was carried out on a sample containing a 500-fold molar excess of nitrate. Previously, the sample had been reduced to a potential of approximately −500 mV, and was then incubated with nitrate for 40 min to produce the nitrate signal with its higher intensity, and was then reoxidized with air. This sample, which shows the nitrate signal, was titrated again with dithionite as explained before. Again, the same redox potential was obtained for the FeS center (Fig. 4), but the *nitrate* signal showed no changes either in intensity

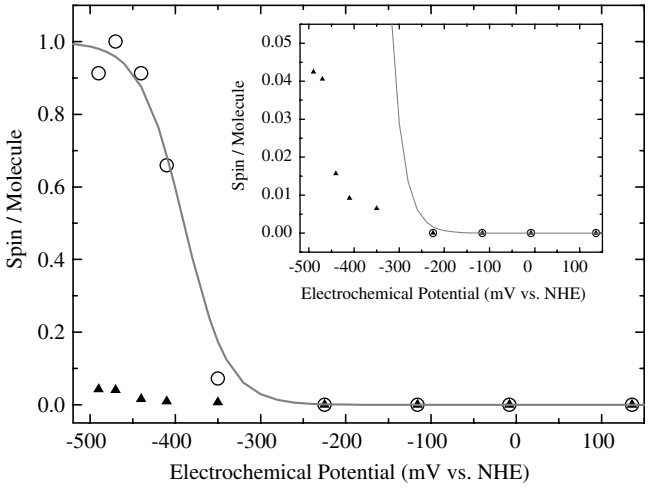

Fig. 3 Redox titrations of *Dd* NapA at room temperature monitored by EPR. *Circles* FeS signal, *triangles* low-potential Mo(V) signal. See "Experimental" for details. The *inset* shows the same data but on a different scale. *NHE* normal hydrogen electrode

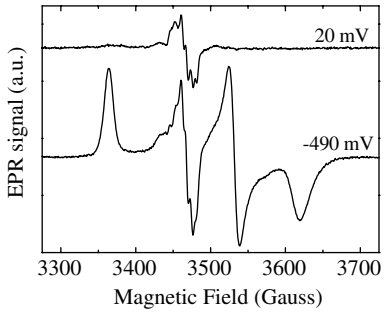

Fig. 4 EPR spectra of a *Dd* NapA sample containing 100 mM of potassium nitrate recorded at 25 K and at 20 and −490 mV (vs. NHE). The full data set at 25 and 100 K is given as supplementary material

or lineshape at 100 K in the range of electrochemical potentials evaluated, which indicates that the nitrate signal is not associated with a redox-active species in the range from 200 to −500 mV. A similar conclusion can be obtained from the analysis of the intensity of the Mo(V) signals at 25 K (the complete set of spectra obtained at 100 and 25 K is given as supplementary material). Figure 4 shows two representative spectra taken at 25 K. Note that the spectra at the potentials where the FeS centers are paramagnetic (e.g., −490 mV) show a slight change in the lineshape of the nitrate signal with respect to those obtained at higher potentials (e.g., 20 mV), indicating a weak magnetic coupling between both centers.

EPR properties of inhibited *Dd* NapA

The EPR properties of *Dd* NapA were evaluated in the presence of cyanide, azide, and perchlorate. The inhibitory effect of cyanide and azide was reported in [26], whereas perchlorate is a competitive inhibitor (unpublished results). Cyanide addition to as-prepared samples of *Dd* NapA does not produce visible changes in the resting Mo(V) (not shown). In contrast, cyanide addition to dithionite-reduced samples followed by reoxidation in air led to the nearly axial signal shown in Fig. 1, spectrum e, which accounts for 0.03 spins per molecule. The same signal was obtained when the sample was exchanged into D_2O, and in samples treated with $KC^{15}N$ ($I_N=1/2$) and $K^{13}CN$ ($I_C=1/2$) (not shown). Furthermore, cyanide addition (KCN, $KC^{15}N$, and $K^{13}CN$) produces only a slight shift to the right of the g_3 value of the FeS signal (Fig. 2, spectrum c), which be originates from conformational changes induced by the cyanide molecule since the EPR data suggest that cyanide is not coordinated to the FeS cluster. Attempts to develop a Mo(V) EPR signal by treating both as-prepared and dithionite-reduced samples with 100-fold molar excess of either sodium azide or potassium perchlorate followed by air oxidation failed to show an EPR signal associated with Mo(V) species.

EPR spectroscopy of *Dd* NapA under catalytic conditions

In contrast to *Pp* NapAB [25], *Dd* NapA has no activity when incubated in the presence of dithionite as the sole electron donor and the enzyme needs reduced MV to be catalytically competent. In a typical kinetics experiment, the enzyme is reacted with MV reduced either with dithionite or with Zn(0) and then the reaction is started by adding nitrate. We performed the EPR experiment using MV reduced with Zn(0) in order to avoid the reaction of the metal centers with the excess of dithionite or their oxidation products. Figure 5 shows the spectra obtained after redox-cycling the enzyme using this procedure. The EPR spectrum of the MV-reduced sample is dominated by a reduced dye radical signal with $g = 2.004$ (Fig. 5, spectrum a). Addition of a 500-fold molar excess of nitrate oxidizes the MV, which becomes colorless, and yields the EPR spectrum shown in Fig. 5, spectrum b. This spectrum is obtained by freezing the sample immediately after nitrate addition and can be obtained as a single signal or as a signal partially overlapped with the EPR signal of the dye. It shows g values and temperature variation typical of Mo(V) ions and can be reasonably simulated assuming hyperfine coupling with a ^{14}N nucleus ($I = 1$, EPR parameters in Table 1). Air oxidation of this sample led to the disappearance of the EPR signal, indicating that this Mo(V) species is redox-active, in contrast to the nitrate signal. Re-reduction of the MV with dithionite in a substoichiometric amount with respect to MV again yields the same signal, because of the excess nitrate present in the mixture. As this signal is obtained under catalytic conditions, it will be called the *turnover* signal. Furthermore, no signals attributable to the paramagnetic $[4Fe–4S]^{+1}$ were detected in this redox cycle of the enzyme.

In order to confirm whether the splitting of the *turnover* signal corresponds to the N atom of the nitrate molecule, the same experiment was conducted with ^{15}N-labeled sodium nitrate ($I_N = 1/2$) (Fig. 5, spectrum c). The spectral analysis was more difficult in this situation, owing to the overlap with a strong free-radical signal. Note that the spectrum c in Fig. 5 was obtained by subtracting the signal of the reduced MV (Fig. 5, spectrum a). The differences found between spectrum b (potassium nitrate with natural abundance isotope composition 99.64% ^{14}N) and spectrum c (^{15}N enriched potassium nitrate; 99%) in Fig. 5 at g_{min} and g_{med} together with the simulation support the possibility that these signals are associated with a Mo(V)–nitrate complex. The discrepancies between the simulation and the experimental spectrum (Fig. 5, spectrum c) at g_{max} are likely due to the inherent uncertainty in the spectral subtraction procedure. More investigations into the variables that govern the origin of the turnover signal will be pursued.

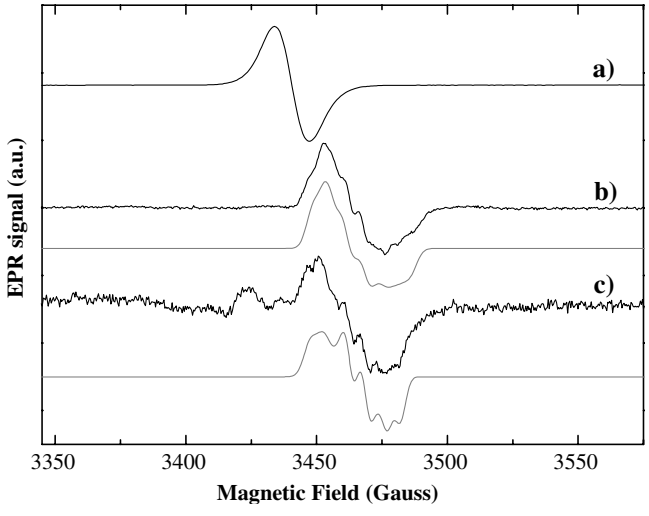

Fig. 5 EPR spectra of the Mo(V) signals of *Dd* NapA obtained in turnover conditions together with the simulation (*gray lines*). *a Dd* NapA reduced with methyl viologen, *b* same as for *a* but after adding 100 mM potassium nitrate, and *c* same as for *a* but after adding 100 mM potassium nitrate labeled with ^{15}N. *c* was obtained by subtracting the signal associated with the reduced dye (the feature at approximately 3,425 G is an artifact obtained from the subtraction procedure). The EPR parameters used in the simulation are given in Table 1. The experimental conditions are as explained in "Experimental" except for the modulation field of 1 G

Discussion

As seen in other Naps [23, 25], *Dd* NapA shows different paramagnetic species: *resting* (Fig. 1, spectrum a), *low-potential* (Fig. 1, spectrum b), *nitrate* (Fig. 1, spectrum c), *high-potential* (Fig. 1, spectrum d), *cyanide* (Fig. 1, spectrum e), and *turnover* signals (Fig. 5, spectrum b). The *nitrate* signal is rhombic and shows a well-defined hyperfine coupling with a nonsolvent exchangeable nucleus with $I = 1/2$. The rhombic character of this signal excludes Mo(V) ion sites having coordination symmetries such as square pyramidal. On the other hand, on the basis of electron–nuclear double resonance studies of *Pp* NapAB [30] and the crystal structure of as-prepared *Dd* NapA [20], it was suggested that the nonsolvent exchangeable hyperfine couplings of the high g (resting) and azide signals in *Pp* NapAB originate from the protons of the β-methylene carbon of the cysteine coordinated to the oxidized Mo site. Since *Dd* NapA and *Pp* NapAB show *nitrate* and high g EPR signals with hyperfine couplings of similar type and magnitude (Table 1), Cys_{140} should be coordinated to this Mo(V) redox state in *Dd* NapA. Therefore, our current interpretation for the *nitrate* species is a distorted six-coordinated site, in which the Mo(V) ion coordinates the four sulfurs of the two pterin cofactors, S_{γ}-Cys_{140} and one sixth ligand, presumably an oxo group (Scheme 1b). This is in contradiction with the structural data taken for the oxidized forms of *Dd* NapA [20] and other closely related enzymes [24], which indicated a hydroxyl/water ligand in the position of the oxo group (Scheme 1a). Additional work is necessary to resolve this discrepancy.

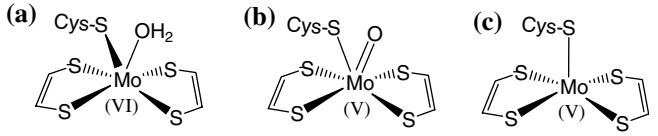

Scheme 1 **a** Coordination around Mo in the oxidized (as-prepared) form of *Desulfovibrio desulfuricans* ATCC 27774 periplasmic nitrate reductase A as determined from X-ray data in [20]. **b** Postulated structures for the nitrate species. **c** Postulated structure for the Mo(V) species giving the cyanide electron paramagnetic resonance signal

As discussed for the *nitrate* signal, the *low-potential* and *high-potential* signals are also anisotropic but have a larger anisotropy than the *nitrate* signal, and the hyperfine structure is not resolved. Given the similarity between these EPR signals and those observed in *Dd* Fdh (Table 1) [28], it is reasonable to assume that the EPR-detectable Mo(V) species are similar in both enzymes. EXAFS studies of oxidized and dithionite-reduced *Dd* Fdh show a distorted six-coordinated Mo site in both redox states [31], suggesting that Cys_{140} is coordinated to Mo in both the *low-potential* and the *high-potential* species. In such a case, the lack of hyperfine structure may be due to greater linewidths and/or noncollinearity of the hyperfine **A** tensor of the proton with respect to the Mo(V) **g** tensor.

The redox properties of the *low-potential* and *nitrate* species are different. Although we could not precisely determine the redox potentials for the *low-potential* species, our data suggest that the redox potentials of the Mo(VI)/Mo(V) and Mo(V)/Mo(VI) couples are lower than −500 mV. In contrast, the *nitrate* Mo(V) species is stable in the range from 200 to −500 mV; therefore, it is evident that nitrate addition to the dithionite-reduced *Dd* NapA modifies the redox properties of the Mo center, resulting in the stable Mo(V) ion *nitrate* species. A substrate-dependent redox potential of the active site have been observed in *Rs* NapAB [32] and in the copper-containing NR from *Pseudomonas chlororaphis* DSM 50135 [33]. In contrast, the redox potential determined for the FeS center is independent of the nitrate, which confirms that the previously discussed redox-potential modulation occurs only at the level of the Mo site. However, despite the influence of nitrate on the redox potential of the Mo center in *Dd* NapA, the *nitrate* species is not linked with the catalytic mechanism of the enzyme. Two results support this hypothesis: (1) *Dd* NapA shows no activity when using dithionite as the sole electron donor, and (2) the *nitrate* species is redox-inactive in the potential range tested.

The fact that nitrate modulates the redox potential of the molybdenum is also suggested in the experiment when the enzyme is in turnover conditions. Incubation of the enzyme with reduced MV ($E^0 = -440$ mV vs. NHE) in the absence of nitrate yields no signal attributable to $[4Fe–4S]^+$ centers, which suggests that Mo is not reduced to the +4 oxidation state. However, nitrate addition to this sample yields the novel *turnover* signal, which indicates that the redox chemistry of the enzyme is changed in the presence of the substrate, and that a fraction of the Mo centers are in the +5 oxidation state when the reduced MV is consumed. The proposed reaction mechanism for NRs implies the binding of the nitrate molecule to the Mo(IV) redox state, which is oxidized to Mo(VI) after nitrate conversion to nitrite (see Fig. 7 in [20]). This mechanism implies that Mo(VI) should be reduced to Mo(IV) after MV addition to bind the nitrate molecule. Recent electrochemistry studies in *Rs* NapAB have proposed that the enzyme– nitrate interaction with the active site can be produced not only with Mo in the +4 redox state but also with it in the +5 state [32]. This result may be in line with the detection of the turnover signal. However, additional work to determine whether this species is associated with a Mo(V)–substrate complex is necessary to confirm this hypothesis.

Cyanide-treated samples of *Dd* NapA yield an EPR signal having nearly axial symmetry (Fig. 1, spectrum e), which suggests a different geometry of coordination for Mo with respect to the previously discussed Mo(V) species. This signal shows a hyperfine splitting with a nonsolvent exchangeable proton (coordination with the cysteine ligand as for the nitrate species). Furthermore, EPR experiments using cyanide with a different isotope composition suggest that cyanide is not coordinated to Mo(V) ions. Mo(V) EPR signals having nearly axial symmetry have been observed in several Mo enzymes with well-documented crystal structures, such as the members of the XO family [4] and formate-reduced *Ec* Fdh-H [34]. The crystal structures of these proteins show Mo sites in square pyramidal coordination, indicating that the Mo(V) site of the *cyanide* species in *Dd* NapA is more compatible with this coordination than distorted hexa coordination (Scheme 1).

The *nitrate* signal resembles those designated as high *g* signals in *Pp* NapAB (*g* values in Table 1) [25, 35], which were assumed to be from a catalytic intermediate. Furthermore, reaction of *Dd* NapA with cyanide yields an EPR signal similar to those observed in the Mo-containing enzymes *Pp* NapAB [25], air-oxidized Nas from *Cyanobacteria* [29], and dithionite-reduced Fdh from *Methanobacterium formicicum* [36] (Table 1), which suggests similar structures for the Mo sites of these enzymes. The *nitrate* and *cyanide* signals in *Dd* NapA seem to be associated with hexa- and penta-coordinated Mo sites, respectively, instead of the proposed hepta-coordinated sites for the high *g* (nitrate) and the very high *g* (cyanide) signals in *Pp* NapAB [25, 37]. Because of the high similitude between the EPR properties of *Pp* NapAB and *Dd* NapA, it is unlikely that the active sites have different coordination geometry; however, no definitive conclusion can be drawn at the present point of the research and additional work is necessary to resolve these discrepancies.

In summary, we have characterized some EPR Mo(V) species and discussed redox properties and possible structures of the paramagnetic species detected in

Dd NapA. The data suggest that the *low-potential* and *nitrate* signals are not relevant in catalysis and that cyanide does not interact with the active site forming an inhibitor–Mo(V) bond. Furthermore, we detected a novel paramagnetic species produced with the enzyme under catalytic conditions. Whether the *turnover* signal is given by a substrate–Mo(V) complex cannot be confirmed with the current results. Additional experiments are necessary to determine the mechanistic role of this species; however, its detection opens new possibilities of research that might help to elucidate the reaction mechanism of these enzymes.

Acknowledgements P.J.G. (SFRH/BD/10825/2002) and M.G.R. (SFRH/BD/10784/2002) thank FCT for a fellowship grant. C.D.B. and J.J.G.M. thank SECYT (Argentina) and GRICES (Portugal) for a bi-national grant. This work was supported by projects EC HPRN-CT-1999-00084, POCTI/1999/BME/35078, and POCTI/1999/BME/36152 in Portugal, and SEPCYT:PICT 2003-06-13872, CONICET PIP 02559/2000, and CAI + D-UNL in Argentina. C.D.B. is a member of CONICET-Argentina.

References

1. González PJ, Correia C, Moura I, Brondino CD, Moura JJG (2006) J Inorg Biochem (in press)
2. Richardson DJ (2000) Microbiology 146:551–571
3. Moreno-Vivian C, Cabello P, Martinez-Luque M, Blasco R, Castillo F (1999) J Bacteriol 181:6573–6658
4. Hille R (1996) Chem Rev 96:2757–2816
5. Grove J, Tanapongpipat S, Thomas G, Griffiths L, Crooke H, Cole J (1996) Mol Microbiol 19:467–481
6. Stolz JF, Basu P (2002) Chembiochem 3:198–206
7. Siddiqui R, Warnecke-Eberz U, Hengsberger A, Schneider B, Kostka S, Friedrich B (1993) J Bacteriol 175:5867–5876
8. Sears HJ, Sawers G, Berks BC, Ferguson SJ, Richardson DJ (2000) Microbiology 146:2977–2985
9. Ellington MJK, Bhakoo KK, Sawers G, Richardson DJ, Ferguson SJ (2002) J Bacteriol 184:4767–4774
10. Ellington MJK, Sawers G, Sears HJ, Spiro S, Richardson DJ, Ferguson SJ (2003) Microbiology 149:1533–1540
11. Gavira M, Roldan MD, Castillo F, Moreno-Vivian C (2002) J Bacteriol 184:1693–1702
12. Ellington MJK, Richardson DJ, Ferguson SJ (2003) Microbiology 149:941–948
13. Bedzyk L, Wang T, Ye RW (1999) J Bacteriol 181:2802–2806
14. Delgado MJ, Bonnard N, Tresierra-Ayala A, Bedmar EJ, Muller P (2003) Microbiology 149:3395–3403
15. Bursakov S, Liu M, Payne WJ, LeGall J, Moura I, Moura JJG (1995) Anaerobe 1:55–60
16. Liu H, Takio S, Satoh T, Yamamoto I (1999) Biosci Biotechnol Biochem 63:530–536
17. Wang H, Tseng C-P, Gunsalus RP (1999) J Bacteriol 181:5303–5308
18. Brondijk T, Nilavongse A, Filenko N, Richardson D, Cole J (2004) Biochem J 379:47–55
19. Stewart V, Lu Y, Darwin AJ (2002) J Bacteriol 184:1314–1323
20. Dias J, Than M, Humm A, Huber R, Bourenkov G, Bartunik H, Bursakov S, Calvete J, Caldeira J, Carneiro C, Moura J, Moura I, Romao MJ (1999) Struct Fold Des 7:65–79
21. Reyes F, Roldan M, Klipp W, Castillo F, Moreno-Vivian C (1996) Mol Microbiol 19:1307–1318
22. Berks B, Richardson D, Robinson C, Reilly A, Aplin R, Ferguson S (1994) Eur J Biochem 220:117–124
23. Arnoux P, Sabaty M, Alric J, Frangioni B, Guigliarelli B, Adriano J, Pignol D (2003) Nat Struct Biol 10:928–934
24. Moura JJG, Brondino CD, Trincao J, Romao MJ (2004) J Biol Inorg Chem 9:791–799
25. Butler C, Charnock J, Bennett B, Sears H, Reilly A, Ferguson S, Garner C, Lowe D, Thomson A, Berks B, Richardson D (1999) Biochemistry 38:9000–9012
26. Bursakov S, Carneiro C, Almendra M, Duarte R, Caldeira J, Moura I, Moura J (1997) Biochem Biophys Res Commun 239:816–822
27. Liu MC, Peck HD Jr (1981) J Biol Chem 256:13159–13164
28. Costa C, Teixeira M, LeGall J, Moura JJG, Moura I (1997) J Biol Inorg Chem 2:198–208
29. Jepson BJN, Anderson LJ, Rubio LM, Taylor CJ, Butler CS, Flores E, Herrero A, Butt JN, Richardson DJ (2004) J Biol Chem 279:32212–32218
30. Butler C, Fairhurst S, Ferguson S, Thomson A, Berks B, Richardson D, Lowe D (2002) Biochem J 363:817–823
31. George GN, Costa C, Moura JJG, Moura I (1999) J Am Chem Soc 121:2625–2626
32. Frangioni B, Arnoux P, Sabaty M, Pignol D, Bertrand P, Guigliarelli B, Leger C (2004) J Am Chem Soc 126:1328–1329
33. Pinho D, Besson S, Brondino CD, de Castro B, Moura I (2004) Eur J Biochem 271:2361–2369
34. Khangulov SV, Gladyshev VN, Dismukes GC, Stadtman TC (1998) Biochemistry 37:3518–3528
35. Bennett B, Berks B, Ferguson S, Thomson A, Richardson DJ (1994) Eur J Biochem 226:789–798
36. Barber MJ, Siegel LM, Schauer NL, May HD, Ferry JG (1983) J Biol Chem 258:10839–10845
37. Bennett B, Charnock J, Sears H, Berks B, Thomson A, Ferguson S, Garner C, Richardson DJ (1996) Biochem J 317:557–563